Received: 10 July 2023 | Revised: 27 October 2023 | Accepted: 24 November 2023

IET Power Electronics

DOI: 10.1049/pel2.12648

The Institution of Engineering and Technology WILEY

ORIGINAL RESEARCH

Component design procedure for LCC-S wireless power transfer systems based on genetic algorithms and sensitivity analysis

Fabio Corti[1] | **Matteo Intravaia**[1] | **Alberto Reatti**[1] | **Francesco Grasso**[1] | **Emanuele Grasso**[2] | **Alicia Triviño Cabrera**[3]

[1]DINFO, University of Florence, Firenze, Italy

[2]Lehrstuhl für Antriebstechnik, Universität des Saarlandes, Saarbrücken, Saarland, Germany

[3]Department of Electrical Engineering, Universidad de Málaga, Málaga, Spain

Correspondence
Fabio Corti, DINFO, University of Florence, Firenze, Italy.
Email: fabio.corti@unifi.it

Abstract

This paper introduces a novel approach for designing a Wireless Power Transfer (WPT) system with LCC-S compensation. Since WPT systems operate under resonant conditions, even small deviations of the components from the nominal values can result in a significant reduction of the power transferred to the load, and in an increment of the circulating currents, reducing the system efficiency. The design techniques available today in the literature provide a unique combination of passive components capable of transferring a certain power to the load. This is a limitation, because, in practice, there are several combinations that allow reaching the desired output power, but they are usually neglected because they are extremely difficult to compute analytically. For this reason, in this paper, the authors present an innovative design procedure that enables, through a Genetic Algorithm, the identification of multiple feasible combinations of the LCC-S components capable of achieving the desired output power. Moreover, the authors evaluate the effects of the component tolerances on the output power to determine which combinations are more robust to component variations. This task is performed by calculating the probability that a particular combination yields the desired output power, once the tolerances have been considered, following a Monte Carlo approach. This information is utilized to decide whether it is possible to reduce the component quality (worsening the tolerance) without affecting the performance. Finally, an optimal solution granting both low-cost and robustness against component tolerances can be individuated. The proposed design procedure is applied to a case study and validated experimentally.

1 | INTRODUCTION

Inductive Wireless Power Transfer (IWPT) enables the transmission of electrical energy through electromagnetic induction between devices. IWPT offers numerous benefits compared to conventional wired charging methods [1]: it eliminates the need for physical connections between the charging device and the power source, resulting in reduced cable wear, enhanced device placement flexibility, and decreased cable clutter [2].

An IWPT system comprises two primary components: a transmitter and a receiver. When the transmitter is linked to an alternating current (AC) power source, it generates an alternating magnetic field. When the receiver is in proximity to the transmitter, the magnetic field induces a voltage, which leads to an AC in the receiver coil to power a load [3, 1]. Since the distance between the primary and the secondary can be up to tens of centimetres, the coupling factor is usually low [4]. To minimize reactive power circulation and enhance transmission efficiency, additional inductors and capacitors are connected to the transmitter and receiver coils. Different resonant compensation circuits can be implemented based on the specific connection configuration.

Several resonant topologies have been proposed over the years. Extensive overviews and comparisons have been proposed in [5–9]. Each topology is characterized by a particular behaviour under load, frequency, and coupling coefficient variations [10]. For instance, the Series-Series (SS) compensation is characterized by high transmission efficiency at low coupling

TABLE 1 Sensitivity analysis for IWPT overview.

Ref.	Topology	Sensitivity analysis
[23]	LCC-S	Analytical. Sensitivity in respect to capacitor variations. Analysis of the input impedance, output power, and efficiency.
[24]	SS	Analytical. Analysis of output voltage transfer function poles and zeros trajectory in respect of load resistance, filter capacitance, and coupling coefficient.
[25]	LCC	Sensitivity of output power and efficiency to parameter variations in the double-sided LCC compensated WPT system. Circuit Simulation. Methods (Spice Model) are used to generate parameter combinations inside the +10% tolerance.
[26]	LCC-S	Analytical. Input impedance and voltage transfer function at different load resistances.
[27]	LCC	Analytical. Input impedance and voltage transfer function at different load resistances. Voltage gain under component variations.
[28]	SP	Analytical. Variation of the voltage gain with respect to resonant components.
[29]	LCC	Analytical. Voltage and current transfer function variation with respect to load resistance and components variations.
[30]	SS	Analytical. Output power with respect to resonant capacitors.

IWPT, inductive wireless power transfer

coefficients and operates approximately as a current source [11]. On the other hand, the LCC-S compensation, which is receiving relevant attention lately, achieves better results at higher coupling coefficients and operates approximately as a voltage source [12]. Each topology exploits the resonance phenomenon: inductances and capacitors are tuned to resonate at a particular frequency, minimizing the reactive power and maximizing the active power transmission [13].

Although several resonant compensation design procedures are available in the literature, their practical realization is not trivial. In fact, in resonant circuits, even small variations in the circuit components can severely affect the frequency response and produce significant variations compared to the nominal behaviour [14]. This situation occurs very often in practice, as not all component values are available on the market. In addition, all the components are characterized by a tolerance and their values may change due to temperature, ageing, and other factors.

To address the significance of this aspect, numerous studies have examined the impact of component variations on system performance. Table 1 provides a literature overview specifically focused on IWPT. This kind of analysis, known as Sensitivity Analysis (SA), allows designers to investigate how deviations from the nominal values influence the circuit performance. It also identifies the components that have the most pronounced effects on system behaviour when subjected to variations. These findings can guide designers in making design choices, such as selecting circuit components, identified as critical, with specific technologies and tolerances.

There are three approaches to perform a SA:

- Circuit simulation software. It exploits circuit simulator tools, such as SPICE (Simulation Program with Integrated Circuit Emphasis). By varying each component in the model, the simulator provides a detailed analysis of how changes in these values affect the circuit behaviour [15–17].
- Analytical calculations. The sensitivity is computed for each component as a closed-form mathematical expression. This method is used for simple circuits that can be analyzed using the basic circuit theory [18, 19].
- Experimental testing. This strategy involves the physical realization of the circuit. The SA is carried out by means of direct measurements on the circuit prototype, while varying the components of interest [20–22].

The choice of the SA method depends on the complexity of the circuit, the accuracy required, and the resources available. Moreover, a combination of these techniques can be adopted to achieve more comprehensive results. Table 1 demonstrates that most papers in the literature employ an analytical approach. However, this approach becomes less effective as the circuit complexity increases. These analyses typically assume the variation of a single component at a time, making it challenging to account for the combined effects of multiple components varying simultaneously and their impact on the system performance.

Consequently, there is a gap in the literature regarding a comprehensive procedure that could assist circuit designers in selecting commercial components to achieve specific performance goals. To address this gap, this paper proposes a tool to guide designers in the practical implementation of resonant compensation for wireless power transfer (WPT). This tool aims at providing practical insights and recommendations to aid designers in achieving desired performance outcomes. Unlike the procedures available in the literature, the proposed method allows the following sequence of operations:

1. Identify multiple combinations of commercial components capable of guaranteeing a desired output power. This task is performed using a discrete Genetic Algorithm (GA). For each component, the nominal value and tolerance are provided.
2. Through a Monte Carlo approach, calculate the probability that a combination of components will provide the desired output power value considering the tolerances. This task is fundamental because it gives the designer an objective idea about the robustness of each solution, indicating the outcomes of a hypothetical large-scale production. As a result of this step, some solutions discovered by the discrete GA may be discarded as they are deemed to be too sensitive to component tolerances.
3. Perform an analytical SA on the identified solutions. This step helps understand how the variation of each component affects the output power. From this information, it is

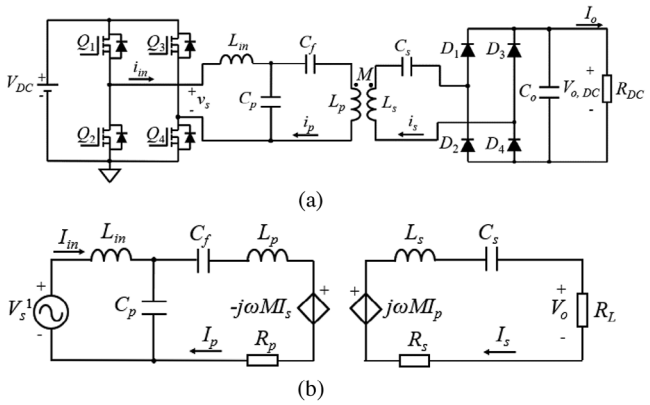

FIGURE 1 LCC-S compensated system. (a) Electrical circuit, (b) FHA equivalent circuit. FHA, first harmonic approximation.

possible to evaluate the possibility of modifying the tolerance of some components. For example, if a component has low sensitivity, it may be convenient to worsen its tolerance (reducing its cost), since its variation would have little effect on the output power. The purpose of this analysis is to optimize the cost of each solution discovered by the second operation. Thus, the final solution individuated by the algorithm is both low-cost and robust against the variations of the components.

Compared to similar works proposing GAs for WPT system design (and, in general, for analog circuit design), our algorithm introduces steps 2 and 3 for guiding the circuit designer not only in selecting the component values to achieve a certain objective (e.g. the output power for a WPT system), but also in optimizing the cost of the circuit realization, without spoiling the performance or, at least, with a precisely quantified deterioration.

This manuscript is organized as follows. In Section 2, the LCC-S compensation is chosen as the case study and the problem related to the design of this topology is described. Furthermore, the proposed tool is presented, and its workflow is illustrated in finer detail. In Section 3, the GA used to explore the space of the possible commercial components that achieve the desired output power is presented. In Section 4, the computation of the probability to reach the desired output power considering the tolerance of the components is shown. In Section 5, the SA calculation is presented. In Section 6, the results of the SA are exploited to optimize the cost of the solutions previously individuated by the GA. In Section 7, an experimental validation is proposed. Finally, Section 8 draws the conclusions.

2 | LCC-S COMPENSATION

2.1 | Circuit analysis

Figure 1a depicts the electrical circuit of a LCC-S compensated IWPT system. As the circuit operates in resonance, the currents and voltages in the resonant tank can be approximated as sinusoidal. This approximation, known as First Harmonic Approximation (FHA), enables the analysis of the circuit to be greatly simplified while maintaining a satisfactory level of accuracy [31, 32].

Under FHA, the square voltage v_s can be approximated as $v_s^1 = (4/\pi)V_{DC}sin(\omega t) = (4/\pi)V_s^1 sin(\omega t)$, as shown in Figure 1b [4]. Using the Kirchhoff's voltage and current laws, the circuit can be modelled as

$$\begin{bmatrix} V_s^1 \\ 0 \\ 0 \end{bmatrix} = \begin{bmatrix} j\left(\omega L_{in} - \frac{1}{\omega C_p}\right) & \frac{j}{\omega C_p} & 0 \\ \frac{j}{\omega C_p} & R_p + j\left(\omega L_p - \frac{1}{\omega C_p} - \frac{1}{\omega C_f}\right) & -j\omega M \\ 0 & -j\omega M & R + j\left(\omega L_s - \frac{1}{\omega C_s}\right) \end{bmatrix} \begin{bmatrix} I_{in} \\ I_p \\ I_s \end{bmatrix} \quad (1)$$

where $R = R_s + R_L$. Inverting (1) and after some manipulations, the output power can be calculated as:

$$P_o = \frac{R_L M^2 V_s^2}{\left(\frac{R}{\omega^2 C_P} - \delta C_P\left(\beta R_p + \gamma R\right)\right)^2 + \left(\frac{\beta}{\omega^2 C_P} + \delta C_P\left(\alpha - \gamma\beta\right)\right)^2} \quad (2)$$

with $\alpha = R_p R + \omega^2 M^2$, $\beta = \omega L_s - 1/(\omega C_s)$, $\delta = \omega L_{in} - 1/(\omega C_p)$, $\gamma = \omega L_p - 1/(\omega C_p) - 1/(\omega C_f)$.

As shown in [23], to cancel the reactive part of the impedance seen by the inverter, the capacitors and the inductors of the resonant tank must be designed according to the following relationship:

$$C_p = \frac{1}{\omega_0^2 L_{in}}, \quad C_f = \frac{1}{\omega_0^2 (L_P - L_{in})}, \quad C_s = \frac{1}{\omega_0^2 L_s} \quad (3)$$

where ω_0 is the angular resonant frequency. Under this condition, the expression of the output power and transmission efficiency can be extremely simplified as

$$\eta = \frac{R_L M^2 \omega_0^2}{R\alpha} \quad (4)$$

$$P_o = \frac{R_L V_S^2 M^2}{R^2 L_{in}^2} \quad (5)$$

Inverting (5), the input inductance L_{in} can be designed to achieve a desired output power in resonant conditions as

$$L_{in} = \frac{V_s \cdot M}{R} \cdot \sqrt{\frac{R_L}{P_o}} \quad (6)$$

Table 2 reports an example of the circuit parameters calculated using Equations (3) and (6). In practice, the commercial

TABLE 2 System parameters.

Parameter	Value
Resonant frequency f_0	85 kHz
Input DC voltage V_{DC}	24 V
Load resistance R_L	50 Ω
Coupling coefficient k	0.36
Primary self-inductance L_p	86.7 μH
Secondary self-inductance L_s	93.5 μH
Primary parasitic resistance R_p	0.82 Ω
Secondary parasitic resistance R_s	0.71 Ω
Nominal output power P_o^{nom}	100 W

TABLE 3 Components values calculated analytically, closer commercial values, and relative errors.

Parameter	Analytical value	Commercial value	Relative error
L_{in}	9.8 μH	10 μH	+2%
C_p	359 nF	330 nF	−8%
		470 nF	+30%
C_f	45.5 nF	33 nF	−27%
		47 nF	+3%
C_s	35.5 nF	33 nF	−7%
		47 nF	+24%

value of the components may be different from the values calculated analytically. The commercial values available on the market depend on the E series of tolerance, defined by the IEC 60063:2015 standard [33]. The E series is a system derived for use in electronic components. It consists of the E3, E6, E12, E24, E48, E96, and E192 series, where the number after the 'E' designates the quantity of logarithmic value steps per decade. Each series corresponds to a tolerance: E3 (40%), E6 (20%), E12 (10%), E24 (5%), E48 (2%), E96 (1%), and E192 (0.5%). For example, Table 3 shows, for the components in the resonant tank, the commercially available E6 values closest to the ones reported in Table 2, with the relative error made when substituting the commercial values to the analytical ones.

In addition, misalignments between the primary and secondary coils can be easily taken into account including a tolerance on the mutual inductance, without any complications in the design procedure. For a simpler analysis, without loss of generality, in this paper the coupling coefficient is assumed to be constant to $k = 0.36$. As shown in Table 2, in this work, the mutual inductance is assumed to be constant. Since the converter operates in resonant conditions, small changes with respect to the calculated values can lead to significant variations of the output power. For example, in Table 4, the output power measured simulating the circuit with the analytical values and the closest commercial values ($L_{in} = 10$ μH, $C_p = 330$ nF, $C_f = 47$ nF, $C_s = 33$ nF) is shown.

TABLE 4 Comparison of the output power for the component values calculated analytically and for the closest commercial values.

Parameter	Value
Calculated values	100 W
Closest commercial values	85 W

As can be seen, although the distance with respect to the analytical value of each component is lower than 20%, the effects on the system performance are significant. From the above analysis it is clear that, even by choosing component values extremely close to the desired values, system performance can be significantly compromised. A partial solution to mitigate this issue can be to choose low tolerance components but this leads to higher costs. Furthermore, other external factors such as ageing, temperature, and humidity can lead to variations in the component values. For this reason, knowing the influence of each component on the behaviour of the system is extremely useful in the design phase. In fact, the knowledge of the effects that a component variation produces on the system performance can be useful to properly choose the most suitable commercial components.

2.2 | Description of the proposed design approach

The design procedure proposed in this paper can be summarized by the flowchart shown in Figure 2. The procedure can be divided into three steps:

- Step I: identification of a given number N of combinations of components $\boldsymbol{S}$ that allow reaching the desired output power within given bounds, $P_o^{min} < P_o < P_o^{max}$. Numerically, infinite combinations exist. Anyway, only few of them are feasible in practice according to the commercial values. Thus, the result of this step is a set of commercial value combinations $\boldsymbol{S} = [S_1; S_2; \ldots; S_N]$ where $S_k = (L_{in}^k, C_f^k, C_p^k, C_s^k)$ with $k = 1, 2, \ldots, N$. Each solution allows reaching the desired output power target within the given range $P_o^{min} < P_o < P_o^{max}$. This task is performed using a discrete GA. These algorithms operate iteratively generating and evaluating a population of candidate designs, exploiting the best ones based on a fitness function, and applying genetic operators such as crossover and mutation to produce new offspring designs. In this step, the component tolerance is completely neglected (see Section 3).
- Step II: once N combinations of component values $\boldsymbol{S}$ have been identified, the effect of the tolerance is studied. This task is performed estimating the probability that a particular solution S_k produces the desired output power. To perform this task the MATLAB Sensitivity Analyzer Toolbox is used. A large number M of combinations ($L_{in}^{k,j}, C_p^{k,j}, C_f^{k,j}, C_s^{k,j}$) with $j = 1, 2, \ldots, M$ are randomly generated according to the tolerance of each component following a Gaussian probability distribution, as specified in the IEC 60063:2015 standard.

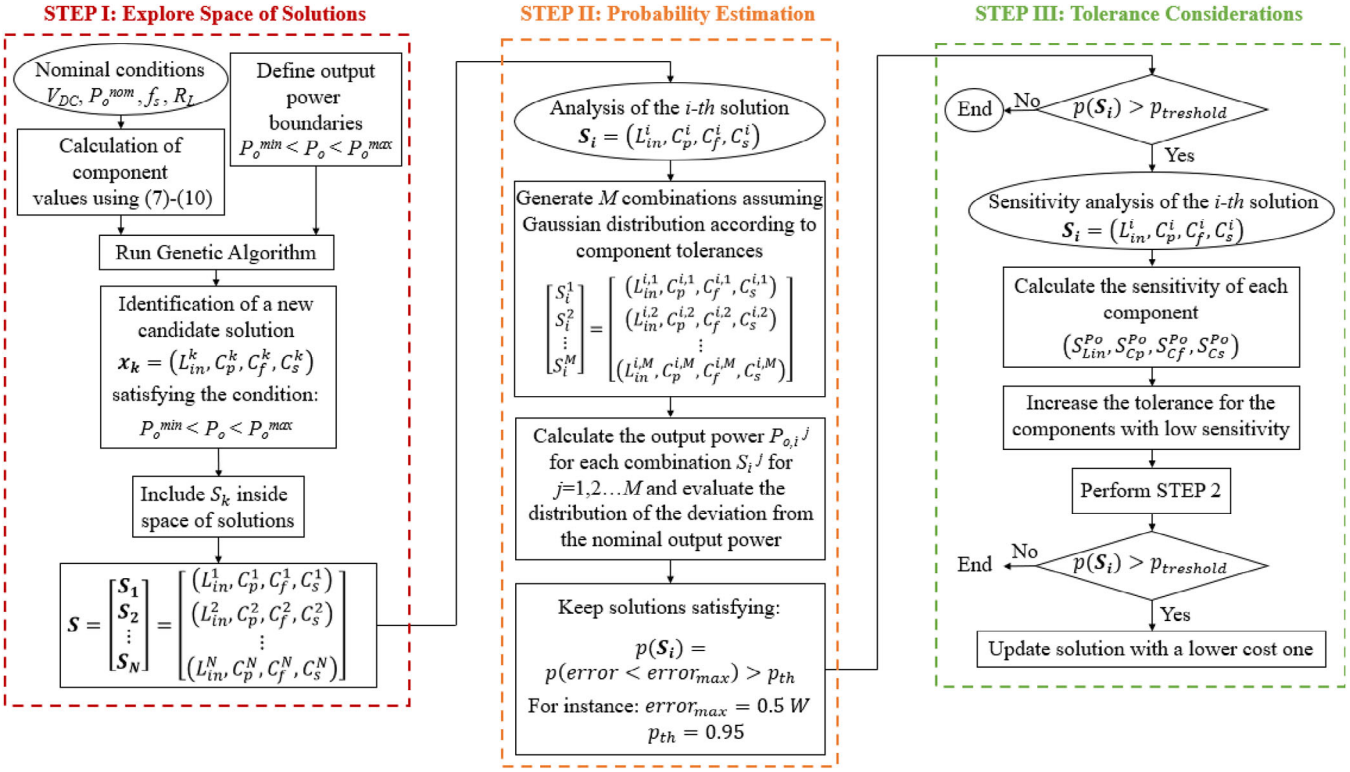

FIGURE 2 Flowchart of the proposed design procedure.

Then, for each combination, the deviation from the nominal output power (i.e. the output power that would be obtained using components having exactly the value calculated for solution S_k) is evaluated. Finally, the probability distribution of this error is calculated and only the solutions satisfying certain confidence conditions are kept, for example, only solutions that produce errors of at most 0.5 W in more than 95% of the cases, considering the tolerances (see Section 4).

- Step III: once a set of possible solutions characterized by high probability of reaching the target is identified, an additional SA is performed. The aim of this step is to understand which components affect the system performance most with their variations. Components that have little influence can be chosen with larger tolerances, while it is more advisable to choose smaller tolerances for those components that have a greater influence on the performance. This step enables us to replace components with reduced tolerances, since, especially for large production volumes, the replacement of even a single component for an alternative with larger tolerance can lead to considerable economic savings (see Sections 5 and 6).

3 | STEP I: INVESTIGATION OF THE SOLUTION SPACE THROUGH GENETIC ALGORITHMS

Optimization problems can be addressed in various ways. GAs have become very popular solutions to optimization tasks. This class of algorithms mimics the Darwinian evolutionary theory, exploiting processes such as crossover, mutation, and natural selection to find the best fitting individual to certain conditions, that is, the optimal solution minimizing an objective function, usually called fitness function. Compared to other strategies, GAs exhibit the ability of solving multiparameter problems, and, additionally, they offer excellent global convergence capabilities [34]. For these reasons, GAs proved to be suitable for those applications where the fitness function typically depends on many circuit components (the problem parameters), usually with large acceptable ranges for their values [35, 36].

In general, a GA involves the following phases:

1. Generation of the initial population: a first pool of individuals is generated. Each individual has a set of genes, which correspond to the problem parameters, selected randomly inside certain limits imposed by the problem constraints.
2. Fitness evaluation: the fitness function is computed for each individual. Such a function reflects the desired target performance; in the case of interest, this can be given in terms of output power, efficiency, cost, or other design specifications.

   Selection: based on the fitness function results, the fittest individuals in the population are selected.
3. Crossover: a new population is generated combining the genes of the previous one. Fitter individuals have better chances to reproduce and get their genes inherited by the next generation.

TABLE 5 GA solution examples, setting 0.5 W as target deviation from the desired output power of 100 W.

Parameter	Solution 1	Solution 2	Solution 3
P_o^{nom} (W)	99.61	100.33	100.23
$F(\boldsymbol{x})$ (W)	0.39	0.33	0.23
L_{in} (μH)/E series	1.91/E96	1.78/E48	10/E24
C_f (nF)/E series	42.2/E96	41.2/E96	38.3/E96
C_s (nF)/E series	78.7/E96	68.1/E96	86.6/E48
C_p (nF)/E series	53.6/E96	110/E24	3.74/E96
TCI	20	17	17

GA, genetic algorithm; TCI, total cost index.

4. Mutation: the genes of the new population undergo random slight variations.
5. Phases 2 to 5 are repeated until an individual achieving the desired characteristics (in terms of fitness) arises, or until a maximum number of iterations is reached.

In our case study, the genes are the values of the circuit components listed in Table 3; therefore, each individual is a four-dimensional vector $\boldsymbol{x} = (L_{in}, C_p, C_f, C_s)$. The fitness function computed on an individual represented by the vector $\boldsymbol{x}$ is given by

$$F(\boldsymbol{x}) = \left|P_o(\boldsymbol{x}) - P_o^{nom}\right| \tag{7}$$

where P_o^{nom} is the target output power determined by the project needs (in this study, fixed at 100 W) and $P_o(\boldsymbol{x})$ is the output power obtained using the combination $\boldsymbol{x}$. When an individual exhibits a fitness function lesser than a given target (i.e. when a combination of components yields an output power closer to the target power than a certain threshold), the algorithm exits presenting that individual as the solution to the optimization problem. In the following, the output power obtained for a solution is indicated as P_o^{nom}. To consider the transmission efficiency, only the solutions with $\eta > 0.9$ are kept.

A peculiarity of optimization techniques applied to circuit design is that the problem variables (i.e. the component values) may be chosen continuously from a given interval only in theory. In fact, the admissible values are restricted to the ones available on the market, resulting in a discrete optimization problem. Thus, the algorithm implemented in this work is a discrete GA: its workflow follows the steps illustrated before, with the exception that the individuals in each generation must have genes taken from a predetermined discrete set of values. Such discrete sets correspond to the E series establishing the available values for electronic components. In practice, the proposed GA initially chooses randomly the E series for the four components L_{in}, C_p, C_f, C_s and, consequently, the possible values for each component are fixed and used as constraints to the generation of the population individuals. Iterating the GA execution, multiple solutions featuring different circuit components taken from different E series can be discovered. Table 5 reports some examples of solutions obtained imposing

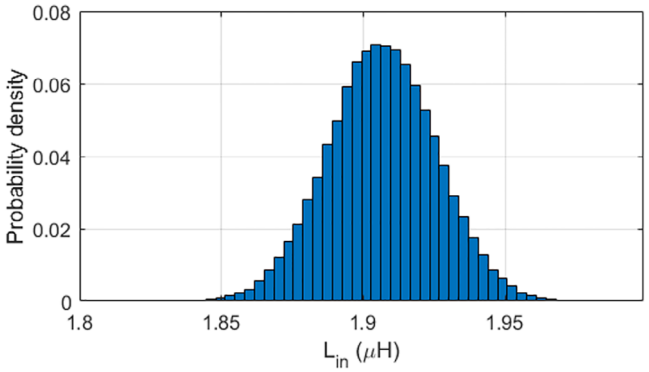

FIGURE 3 Probability distribution of the inductor value considering a 1% tolerance around the nominal value of 1.91 μH.

99.5 W < $P_o(\boldsymbol{x})$ < 100.5 W.

Since components with tighter tolerances cost more, a Total Cost Index (*TCI*) has been introduced, as shown in Table 5. This latter is an indicator of the solution cost. The following Cost Index (*CI*) parameters have been assigned: $CI_{E192} = 6$, $CI_{E96} = 5$, $CI_{E48} = 4$, $CI_{E24} = 3$, $CI_{E12} = 2$, $CI_{E6} = 1$, $CI_{E3} = 0$. The TCI is obtained as the summation of the cost indices of the single components. As explained in Section 6, the TCI is the starting point for further optimization of each solution.

4 | STEP II: COMPONENT TOLERANCE

Electric components are characterized by tolerance. As already mentioned in Section 2, this aspect is particularly critical, since even small deviations of the components from the nominal values can result in low output power transmission for the LCC-S compensation. For this reason, the effect of component tolerances on the output power needs to be investigated in depth.

The values that an electric component with a given tolerance can assume can be modelled by a Gaussian probability distribution. The mean μ is the nominal value of the component while the standard deviation σ is equal to the tolerance [37].

For example, in Figure 3, the probability distribution (50,000 values were taken) obtained considering the tolerance for the inductor value found in Solution 1 of Table 5 is shown. Since the inductor is from E96 series, a 1% tolerance is considered, yielding a standard deviation of σ = 19.1 nH, with a mean of μ = 1.91 μH. Similar distributions are obtained for the other components.

At this point, it is possible to draw from these distributions arbitrarily large sets of values and compute for each combination $\boldsymbol{x}$ the output power $P_o(\boldsymbol{x})$. For each combination, the absolute value of the error on the output power can be calculated as

$$e(\boldsymbol{x}) = \left|P_o(\boldsymbol{x}) - P_o^{nom}\right| \tag{8}$$

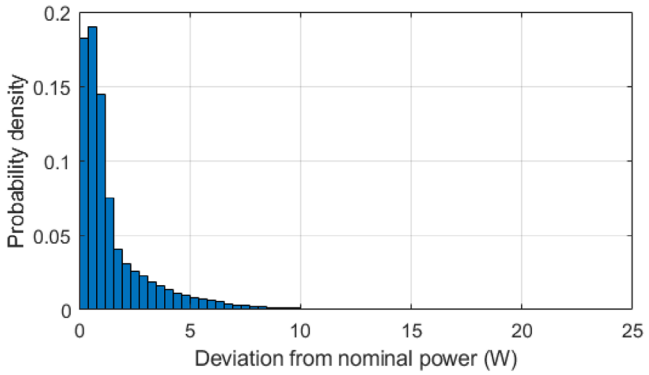

FIGURE 4 Probability distribution of the deviation from the nominal output power, given by Equation (9), due to component tolerances for solution 1 of Table 5.

TABLE 6 $p_{10\%}$, $p_{5\%}$, and $p_{1\%}$ calculated using the frequentist approach on the solutions of Table 5.

Parameter	Solution 1	Solution 2	Solution 3
$p_{10\%}$	0.997	0.998	0.991
$p_{5\%}$	0.943	0.965	0.924
$p_{1\%}$	0.464	0.566	0.519

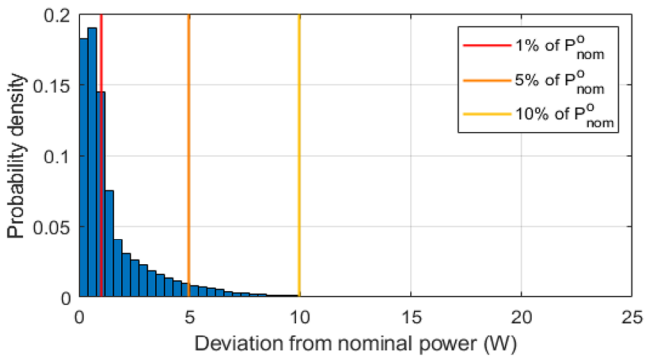

FIGURE 5 Probability distribution of the deviation from the nominal output power, given by Equation (12), due to component tolerances for solution 1 of Table 5. The coloured lines indicate the limits given by 10%, 5%, and 1% of P_o^{nom}.

Computing (8) for all the component values, the probability distribution shown in Figure 4 is obtained. Since this probability density does not follow any known distribution, a frequentist approach is adopted to calculate three probabilities, namely the probability to have an error on the output power lower than 10% of the nominal power P_o^{nom}, lower than 5% of P_o^{nom}, and lower than 1% of P_o^{nom}, indicated respectively as $p_{10\%}$, $p_{5\%}$, and $p_{1\%}$. As an example, Table 6 reports these probabilities calculated for the solutions of Table 5, considering for each component the appropriate tolerance as determined by the GA.

It is interesting to observe that the distribution of the output power error changes significantly from one solution to another, and therefore the three probabilities, introduced in Table 6, vary as well. For instance, Figure 5 reports the distribution of the

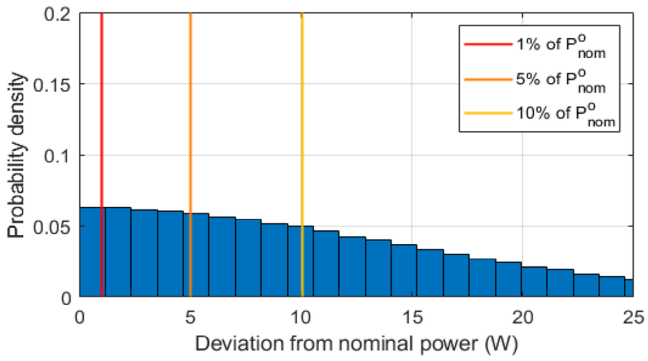

FIGURE 6 Probability distribution of the deviation from the nominal output power, given by Equation (12), due to component tolerances, for another solution individuated by the GA. The coloured lines indicate the limits given by 10%, 5%, and 1% of P_o^{nom}. GA, genetic algorithm.

first solution of Table 5, as already shown in Figure 4, with the indication of the limits given by 10%, 5%, and 1% of P_o^{nom}. In this case, $p_{10\%}$ is nearly 100%, and, consequently, most samples fall to the left of the limit marked with the yellow line. Conversely, Figure 6 shows the output error distribution for another solution, for which the calculated $p_{10\%}$ is only around 50%. This reflects in a completely different probability distribution of $e(\boldsymbol{x})$, much more stretched than the previous case, with the 10% of P_o^{nom} limit (indicated by the yellow line) exceeded by half the instances.

These differences in the solutions found by the GA are due to the multi-variable function linking the output power to the four circuit components L_{in}, C_f, C_s, C_p, that is, the expression reported in Equation (5). Such a function presents a complex shape, characterized by multiple minima; in fact, the GA finds many possible solutions, which grow in number as the components can assume finer values. Although all these solutions approach the target output power with the required precision (0.5 W in this study), not all the solutions 'behave' in the same way. In other terms, the function $P_o(\boldsymbol{x})$ can be extremely different in the neighbourhood of different solutions. As a result, the partial derivatives of $P_o(\boldsymbol{x})$ with respect to the four circuit components, in the neighbourhood of the nominal solution P_o^{nom}, can be extremely different. These topological aspects are investigated in Sections 5 and 6 by means of an SA.

As detailed in Section 6, this kind of studies can be useful to perform a further optimization of the solutions found by the GA. The main idea is that, if a component presents a low sensitivity in a solution, then it might be possible to reduce its E series without affecting not only the nominal output power, but also the probability distribution of $e(\boldsymbol{x})$ due to the tolerance. This would translate into a reduction of the circuit realization cost, improving the *TCI* introduced in Table 5.

5 | STEP III: SENSITIVITY ANALYSIS FOR TOLERANCE SELECTION

SA is an analytical approach used to examine the behaviour of a given system when subjected to changes in its input variables. By

changing the parameters of a model, SA can help determine the impact of these changes on the system output. This technique is particularly valuable in power supply design due to the tolerance inherent in component values, such as resistors, capacitors, and inductors.

From the mathematical point of view, the sensitivity of a parameter a, for example, the output power, with respect to the variation of another parameter b, for example, an inductance or capacitor value, can be expressed by the relationship

$$S_b^a = \lim_{\Delta b \to 0} \left(\frac{\frac{\Delta a}{a}}{\frac{\Delta b}{b}} \right) = \frac{\partial a}{\partial b} \frac{b}{a} \tag{9}$$

When the sensitivity is positive $S_b^a > 0$, an increment of the value b produces an increment of the parameter a. On the other hand, when the sensitivity is negative $S_b^a < 0$, an increment of the value b produces a decrement of the parameter a.

In this section, the sensitivity of the output power P_o in respect of the resonant tank components L_{in}, C_f, C_p, and C_s, is derived analytically. In Section 3, three different solutions have been identified for our case under study. The first solution is characterized by a higher *TCI*, since it uses only E96 tolerance series components. For this reason, in this section, the SA for this solution is carried out, to identify the components that most influence the output power and evaluate the possibility of reducing the tolerance of those characterized by low sensitivity.

5.1 | Effects of primary inductance variation S_{Lin}^{Po}

Using (A1) to (5), the sensitivity of the output power P_o with respect to the input inductance L_{in} can be derived as

$$S_{L_{in}}^{P_o} = 2L_{in} \left(\frac{C_s^2 R_L^2 \omega^2 \sigma_5 \left(\sigma_1 \sigma_5 - \omega^2 \sigma_2 \left(C_f + C_p - \sigma_6 \right) \right) + \sigma_4 \left(\sigma_1 \sigma_4 - \omega^2 \sigma_2 \sigma_3 \right)}{C_s^2 R_L^2 \omega^2 \sigma_5^2 + \sigma_4^2} \right) \tag{10}$$

where the coefficients are listed in the Appendix. The curves of the sensitivity and the output power for using the first solution reported in Table 5 are shown in Figure 7a.

5.2 | Effects of primary capacitance variation SCpPo

Using (A1) to (5), the sensitivity of the output power P_o with respect to the primary capacitance C_p can be derived as

$$S_{C_p}^{P_o} = 2C_p \left(\sigma_{11} - \frac{\sigma_2 L_{in} \omega^2 \left(\sigma_{12} \sigma_{13} + C_s^2 \omega^8 \left(\sigma_9 - 1 \right) \sigma_5 \right)}{C_s^2 R_L^2 \omega^2 \sigma_5^2 + \sigma_{13}^2} \right) \tag{11}$$

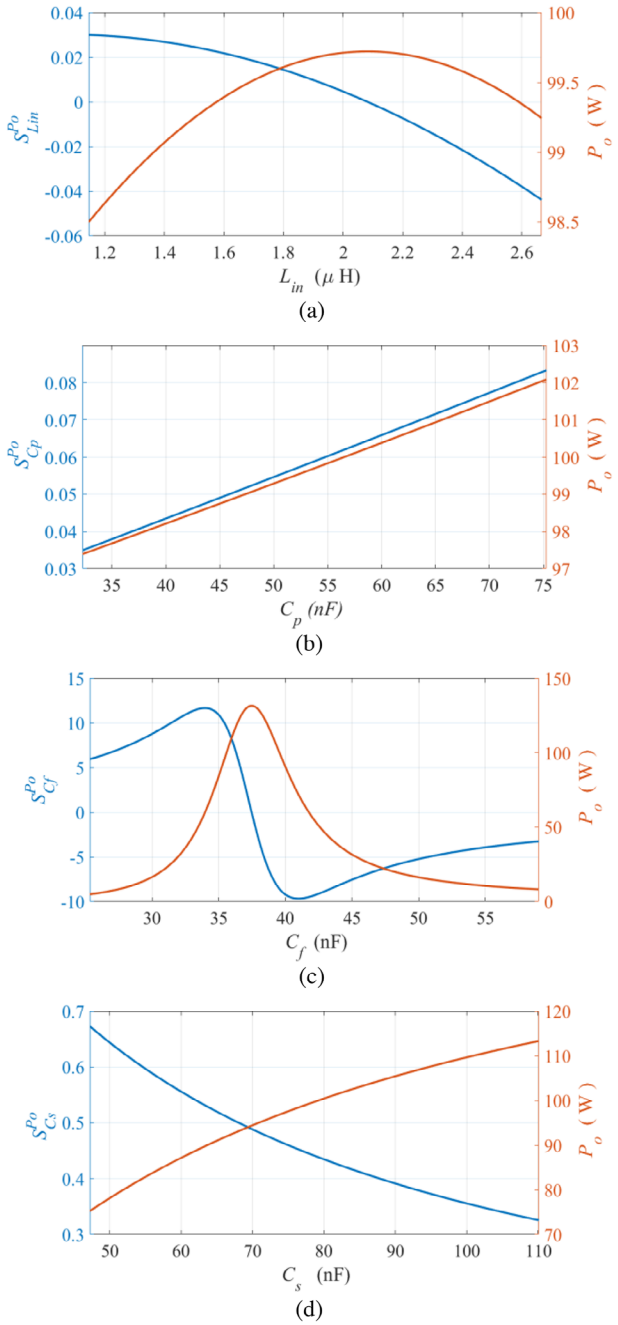

FIGURE 7 Effects of component variations: sensitivity (blue) and output power (red). (a) Input inductance L_{in}. (b) Primary capacitance C_p. (c) Filtering capacitance C_f. (d) Secondary capacitance C_s.

where the coefficients are listed in the Appendix. The curves of the sensitivity and the output power for using the first solution reported in Table 5 are shown in Figure 7b.

5.3 | Effects of filter capacitance variation S_{Cf}^{Po}

Using (A1) to (5), the sensitivity of the output power P_o with respect to the secondary capacitance C_f can be derived as

$$S_{Cf}^{Po} = 2\left(\frac{C_s^2 R_L^2 \omega^2 \sigma_5^2 \left(1 - C_f\left(\sigma_{18}\sigma_{19} + \omega^2\left(L_{in} + L_p - \sigma_6\right)\right) + C_f\left(\omega^2\sigma_{20}\sigma_4 - \sigma_{18}\sigma_{19}\sigma_4^2\right) + \sigma_4\right)}{C_s^2 R_L^2 \omega^2 \sigma_5^2 + \sigma_4^2}\right) \tag{12}$$

where the coefficients are listed in the Appendix. The curves of the sensitivity and the output power for using the first solution reported in Table 5 are shown in Figure 7c.

5.4 | Effects of secondary-side capacitance variation S_{Cs}^{Po}

Using (A1) to (5), the sensitivity of the output power P_o with respect to the secondary capacitance C_s can be derived as

$$S_{Cs}^{Po} = 2C_s\left(\frac{C_s R_L^2 \omega^2 \sigma_5 \left(2\sigma_{15} - C_s\sigma_{14}\right) + \sigma_{17}\left(\sigma_{14} - \sigma_{15}\sigma_{16}\right)}{\sigma_2\left(C_s^2 R_L^2 \sigma_5 + \sigma_{17}^2\right)}\right) \tag{13}$$

where the coefficients are listed in the Appendix. The curves of the sensitivity and the output power for using the first solution reported in Table 5 are shown in Figure 7d.

6 | STEP III: TCI OPTIMIZATION

The last step of the presented algorithm is the optimization of the *TCI* parameter introduced in Table 5. The *TCI* is linked to the E series of the selected circuit components and, consequently, to the cost of the components themselves. A higher *TCI* corresponds to a higher overall circuit realization cost. Since the GA does not take into consideration this aspect, each solution individuated at step I of the proposed design procedure undergoes a further optimization stage that tries to minimize the *TCI*. To this aim, the SA performed in Section 5 is adopted to establish which components the output power is less sensitive to; the algorithm then tries to reduce the E series of the components having lower sensitivity, choosing the closest value belonging to the previous E series. Thus, a new solution is produced and evaluated in terms of output power accuracy and of the distribution of the error $e(\boldsymbol{x})$, in particular of the three probabilities $p_{10\%}$, $p_{5\%}$, and $p_{1\%}$ introduced at step II. If the new solution satisfies certain conditions (which do not need to be the same constraints imposed on the GA, depending on the necessity of the designer), it is substituted into the current solution. This process iterates until none of the components admits a further E series reduction without exceeding the imposed constraints.

As an illustrative example, Table 7 reports the *TCI* optimized solutions of Table 5. For Solution 1, the algorithm was able to reduce the E series of the L_{in} inductor from E96 to E12, of the C_s capacitor from E96 to E48, and of the C_p capacitor from E96 to E12, while the C_f capacitor stayed the same. Thus, the *TCI* dropped from 20 to 13. Besides, the three probabilities were not affected appreciably. Similar considerations can be made for the other two solutions.

These results are perfectly justified and in line with what given by the SA. Taking as an example solution 1, the inductor sensitivity in the neighbourhood of the solution (Figure 7a) is low, which translates in an almost flat region of the P_o curve (red line in Figure 7a); therefore, the algorithm was able to reduce considerably the inductor E series without affecting the performance. Similarly, from Figure 7b, the capacitor C_p could be reduced to E12 series. On the other hand, the C_f and C_s capacitors could not be improved, since they present higher sensitivities, especially the C_f capacitor, causing strong output power variations, for example, Figures 7c and 7d.

Given the results in Table 7, Solution 1 appears to be the most attractive, having lower cost ($TCI = 13$) and higher $p_{10\%}$ and $p_{5\%}$ probabilities compared to Solution 3, while we could rule

TABLE 7 GA solutions presented in Tables 5 and 6, modified to optimize the *TCI* parameter.

Parameter	Solution 1	Solution 2	Solution 3
P_o^{nom} (W)	99.78	100.50	99.99
$F(\boldsymbol{x})$ (W)	0.22	0.50	0.01
L_{in} (μH)/E series	1.8/E12	1.8/E24	10/E24
C_f (nF)/E series	42.2/E96	41.2/E96	38.3/E96
C_s (nF)/E series	78.7/E48	68.1/E48	86.6/E48
C_p (nF)/E series	56.0/E12	110/E24	3.3/E6
TCI	13	15	13
$p_{10\%}$	0.997	0.998	0.990
$p_{5\%}$	0.944	0.962	0.921
$p_{1\%}$	0.428	0.460	0.492

GA, genetic algorithm; TCI, total cost index.

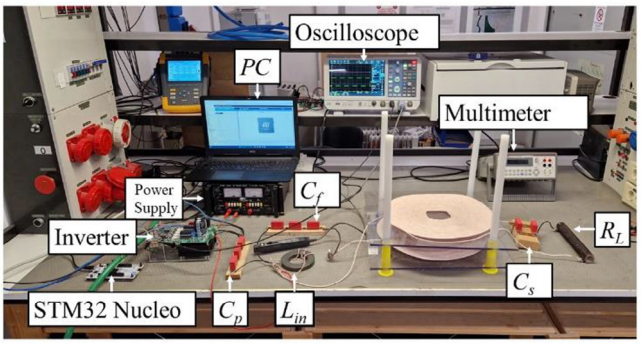

FIGURE 8 Experimental setup of LCC-S compensated WPT. WPT, wireless power transfer.

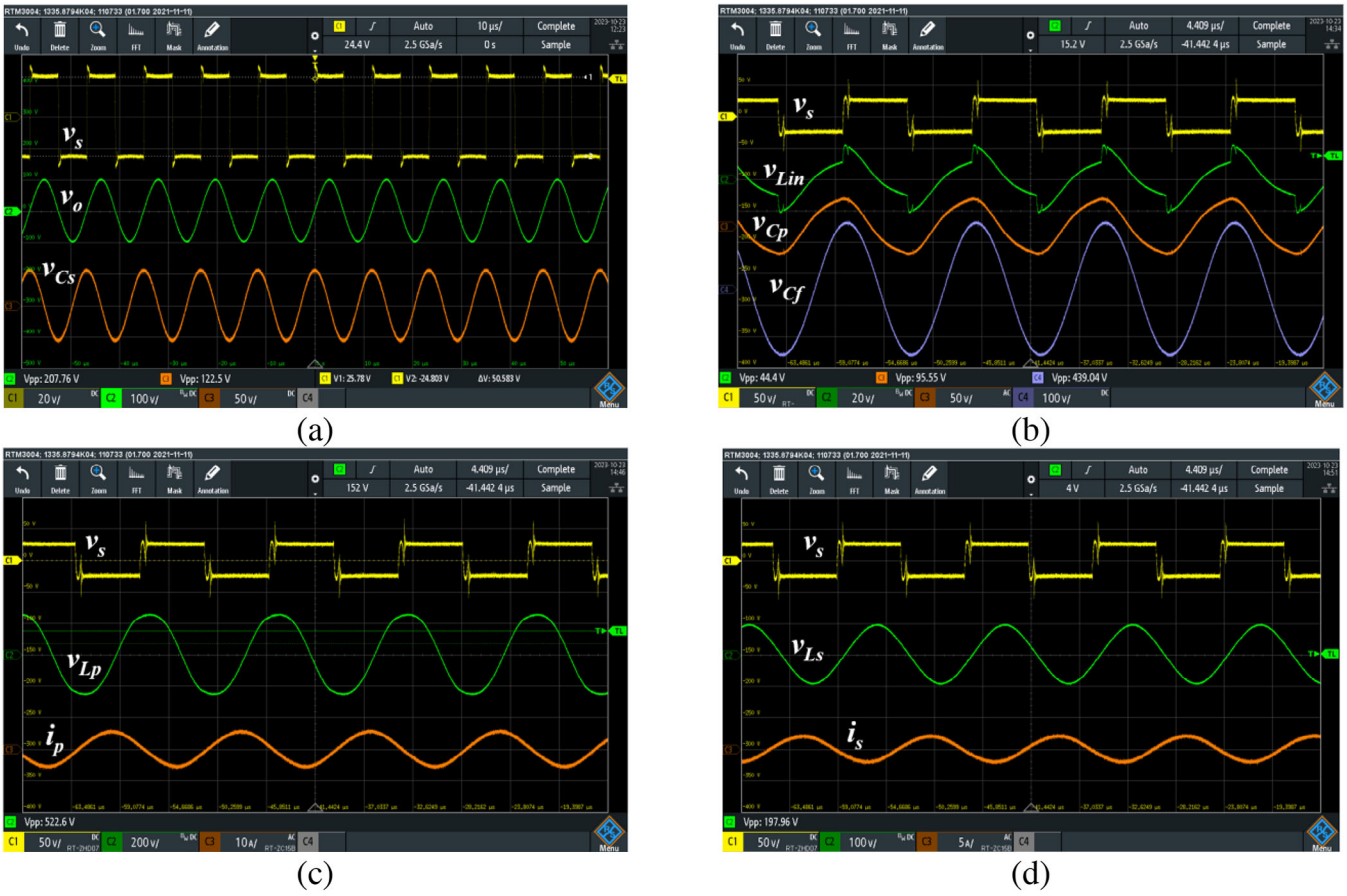

FIGURE 9 Experimental measured currents and voltages on the main circuit components for Solution 1.

out Solution 2 because of its higher *TCI*. Note that, in practical cases, defining the optimal solution may not be straightforward, as the final choice of which configuration to implement depends on the designer's needs. For example, a higher *TCI* solution might result preferable if the selected components were already available at stock; in other instances, the designer may be willing to sacrifice cost to achieve extremely high performance. In general, many metrics can be considered to compare different circuit configurations [38]. In this work, the *TCI* has been selected as the main indicator for comparing different solutions, but, depending on the application, different metrics can be chosen according to the priorities of the designer.

7 | EXPERIMENTAL VALIDATION

To evaluate the performance of the solutions in Table 7, the experimental setup shown in Figure 8 has been implemented.

The inductor has been realized using a core 5977001621 by Fair-Rite and a Litz wire made up by 12,640 strands AWG 38. The capacitors have been realized connecting in series/parallel capacitors with $C = 33$ nF (SNFP X0 2330 7D 4A KS00 by WIMA, E6 20% tolerance) and $C = 1.5$ µF (B32714H2155K000 by EPCOS/TDK, E12 10% tolerance). The measured values for the three solutions are shown in Table 8.

TABLE 8 Measured components values and external series resistance (ESR).

Parameter	Solution 1	Solution 2	Solution 3
L_{in} / ESR	1.62 µH/7 mΩ	1.87 µH/13 mΩ	9.6 µH/89 mΩ
C_f / ESR	41.8 nF/31 mΩ	41.4 µH/32 mΩ	38.6 µH/52 mΩ
C_s / ESR	79.3 nF/23 mΩ	67.0 µH/67 mΩ	85.5 µH/41 mΩ
C_p / ESR	61.2 nF/27 mΩ	112.8 µH/24 mΩ	2.7 µH/19 mΩ

Using the values listed in Table 8, the circuit shown in Figure 1b has been created experimentally, as shown in Figure 8. The current/voltage stresses on each component are summarized in Table 9.

As shown in Table 9, the difference in terms of voltage stresses on the components does not change significantly depending on the different solutions. Thus, the choice of one solution rather than another is not characterized by significant cost variations due to the choice of components characterized by higher voltage or current ratings. The current/voltage waveforms on the main components are shown in Figure 9 for Solution 1. Regarding the conversion efficiency, the experimentally measured output power and transmission efficiency for each solution are shown in Table 10.

TABLE 9 Component stresses.

Parameter	Solution 1	Solution 2	Solution 3
V_{Lin}^{max} / I_{Lin}^{max}	24 V/7.4 A	25 V/8.5 A	40 V/6 A
V_{Cp}^{max} / I_{Cp}^{max}	47 V/4.5 A	52 V/5.5 A	63 V/0.7 A
V_{Cf}^{max} / I_{Cf}^{max}	256 V/5.7 A	255 V/5.6 A	277 V/5.7 A
V_{Lp}^{max} / I_{Lp}^{max}	275 V/5.7 A	250 V/5.6 A	291 V/5.7 A
V_{Ls}^{max} / I_{Ls}^{max}	99 V/1.9 A	104 V/2.1 A	96 V/1.8 A
V_{Cs}^{max} / I_{Cs}^{max}	41 V/1.9 A	49 V/2.1 A	37 V/1.8 A

TABLE 10 Measured output power and efficiency.

Parameter	Solution 1	Solution 2	Solution 3
P_o (W)	95.7	104.3	97.2
η	94.3	93.9	93.7

As it can be seen, each solution allows the achievement of the desired power within a tolerance of 10%. As previously mentioned, the conversion efficiency is approximately constant independently of the solution. The variation in efficiency is mainly due to the parasitic resistances of the components rather than to the values of the capacitances and inductances.

8 | CONCLUSION

In this paper, a tool to guide circuit designers in the practical implementation of resonant compensation for WPT systems is proposed. This tool aims to provide practical insights and recommendations to aid designers in achieving desired performance outcomes. The developed algorithm applies a GA to individuate combinations of components that achieve the required output power to be transferred on the load. Then, considering the component tolerances, the probability that a particular solution allows to actually reach the expected output power is estimated. Only solutions granting high success probabilities are kept as acceptable. Finally, an SA, performed for each configuration, provides information for decreasing the E series of the components having less influence on the output power with the aim of reducing the costs. Therefore, the algorithm outputs a set of possible solutions exhibiting low cost and low sensitivity to component variations. The designer has the task of selecting the most suitable configuration from the proposed options to meet the project requirements. An experimental validation of the method is also presented in the last section of this paper, confirming that the procedure allows reaching the desired output power in a WPT system. As a future development, the effects of misalignment will be taken into account for the optimal design of the compensation circuit. This aspect is of fundamental importance when dealing with dynamic WPT (e.g. applications for electric mobility), where the coupling coefficient varies continuously during the system operation.

AUTHOR CONTRIBUTIONS

Fabio Corti: Writing—review & editing. **Matteo Intravaia**: Writing—review & editing. **Alberto Reatti**: Writing—review & editing. **Francesco Grasso**: Writing—review & editing. **Emanuele Grasso**: Writing—review & editing. **Alicia Triviño**: Writing—review & editing.

CONFLICT OF INTEREST STATEMENT

The authors declare no conflict of interest.

DATA AVAILABILITY STATEMENT

Research data are not shared.

ORCID

Fabio Corti https://orcid.org/0000-0001-8888-0388
Francesco Grasso https://orcid.org/0000-0002-8697-2091
Alicia Triviño Cabrera https://orcid.org/0000-0002-7516-2878

REFERENCES

1. Tran, M.T., Thekkan, S., Polat, H., Tran, D.-D., El Baghdadi, M., Hegazy, O.: Inductive wireless power transfer systems for low-voltage and high-current electric mobility applications: Review and design example. Energies 16(7), 2953 (2023). https://doi.org/10.3390/en16072⟨3:hyphenbreak⟩⟨/3:hyphenbreak⟩953
2. Corti, F., Reatti, A., Nepote, A., Pugi, L., Pierini, M., Paolucci, L., Grasso, F., Grasso, E., Nienhause, M.: A secondary-side controlled electric vehicle wireless charger. Energies 13(24), 6527 (2020). https://doi.org/10.3390/en13246527
3. Detka, K., Górecki, K., Ptak, P.: Model of an air transformer for analyses of wireless power transfer systems. Energies 16(3), 1391 (2023). https://doi.org/10.3390/en16031391
4. Locorotondo, E., Corti, F., Pugi, L., Berzi, L., Reatti, A., Lutzemberger, G.: Design of a wireless charging system for online battery spectroscopy. Energies 14(1), 218 (2021). https://doi.org/10.3390/en14010218
5. Rayan, B.A., Subramaniam, U., Balamurugan, S.: Wireless power transfer in electric vehicles: A review on compensation topologies, coil structures, and safety aspects. Energies 16(7), 3084 (2023). https://doi.org/10.3390/en16073084
6. Zhang, W., Mi, C.C.: Compensation topologies of high-power wireless power transfer systems. IEEE Trans. Veh. Technol. 65(6), 4768–4778 (2016). https://doi.org/10.1109/TVT.2015.2454292
7. Mahesh, A., Chokkalingam, B., Mihet-Popa, L.: Inductive wireless power transfer charging for electric vehicles–a review. IEEE Access 9, 137667–137713 (2021). https://doi.org/10.1109/ACCESS.2021.3116678
8. Venkatesan, M., Rajamanickam, N., Vishnuram, P., Bajaj, M., Blazek, V., Prokop, L., Misak, S.: A review of compensation topologies and control techniques of bidirectional wireless power transfer systems for electric vehicle applications. Energies 15(20), 7816 (2022). https://doi.org/10.3390/en15207816
9. Okasili, I., Elkhateb, A., Littler, T.: A review of wireless power transfer systems for electric vehicle battery charging with a focus on inductive coupling. Electronics 11(9), 1355 (2022). https://doi.org/10.3390/electronics11091355
10. Solouma, N.H., Kassahun, H.B., Alsharafi, A.S., Syed, A., Gardner, M.R., Alsharafi, S.S.: An efficient design of inductive transmitter and receiver coils for wireless power transmission. Electronics 12(3), 564 (2023). https://doi.org/10.3390/electronics12030564
11. Zhu, Y., Wu, H., Li, F., Zhu, Y., Pei, Y., Liu, W.: A comparative analysis of S-S and LCCL-S compensation for wireless power transfer with a wide range load variation. Electronics 11(3), 420 (2022). https://doi.org/10.3390/electronics11030420
12. Zhang, L., Li, H., Guo, Q., Xie, S., Yang, Y.: Research on constant voltage/current output of LCC–S envelope modulation wireless power

transfer system. Energies 15(4), 1562 (2022). https://doi.org/10.3390/en15041562
13. Luca, P., Reatti, A., Corti, F., Mastromauro, R.A.: Inductive power transfer: Through a bondgraph analogy, an innovative modal approach. In: 2017 IEEE International Conference on Environment and Electrical Engineering and 2017 IEEE Industrial and Commercial Power Systems Europe (EEEIC /I&CPS Europe), Milan, Italy, pp. 1–6 (2017). https://doi.org/10.1109/EEEIC.2017.7977737
14. Buu, O.: Sensitivity analysis of resonant circuits. arXiv (2015). http://arxiv.org/abs/1506.00632
15. Corti, F., Reatti, A., Patrizi, G., Ciani, L., Catelani, M., Kazimierczuk, M.K.: Probabilistic evaluation of power converters as support in their design. IET Power Electron. 13(19), 4542–455030 (2020). https://doi.org/10.1049/iet-pel.2020.0828
16. Owen, H., Wilson, T., Feng, S., et al.: A computer-aided design procedurefor flyback step-up DC-to-DC converters. IEEE Trans. Magn. 8(3), 289–291 (1972). https://doi.org/10.1109/TMAG.1972.1067294
17. Cirimele, V., et al.: Uncertainty quantification for SAE J2954 compliant static wireless charge components. IEEE Access 8, 171489–171501 (2020). https://doi.org/10.1109/ACCESS.2020.3025052
18. Zhou, D., Wang, H., Blaabjerg, F.: Mission profile based system-level reliability analysis of DC/DC converters for a backup power application. IEEE Trans. Power Electron. 33(9), 8030–8039 (2018)
19. Wang, H., Liserre, M., Blaabjerg, F., et al.: Transitioning to physics-of-failure as a reliability driver in power electronics. IEEE J. Emerg. Sel. Top Power Electron. 2(1), 97–114 (2014)
20. Yang, S., Bryant, A., Mawby, P., et al.: An industry-based survey of reliabilityin power electronic converters. In: 2009 IEEE Energy Conversion Congress and Exposition, San Jose, CA, pp. 3151–3157 (2009)
21. Villar-Piqué, G., Bergveld, H.J., Alarcón, E.: Survey and benchmark of fully integrated switching power converters: Switched-capacitor versus inductive approach. IEEE Trans. Power Electron. 28(9), 4156–4167 (2013). https://doi.org/10.1109/TPEL.2013.2242094
22. Report of a survey on the performance of shunt capacitors. Trans. Am. Inst. Electr. Eng. 68(2), 1200–1207 (1949). https://doi.org/10.1109/T-AIEE.1949.5060074
23. Bo, Q., Zhang, Y., Guo, Y., Wang, L., Liu, Z., Li, S.: Sensitivity analysis to parameter variations in LCC-S compensated inductive power transfer systems. In: 2020 IEEE PELS Workshop on Emerging Technologies: Wireless Power Transfer (WoW), Seoul, South Korea, pp. 233–237 (2020). https://doi.org/10.1109/WoW47795.2020.9291274
24. Yang, M.: A case study of parametric sensitivity analysis of inductive wireless power transfer system. In: 2021 IEEE 12th Energy Conversion Congress & Exposition—Asia (ECCE-Asia), Singapore, Singapore, pp. 475–478 (2021). https://doi.org/10.1109/ECCE-Asia49820.2021.9479332
25. Lu, F., Hofmann, H., Deng, J., Mi, C.: Output power and efficiency sensitivity to circuit parameter variations in double-sided LCC-compensated wireless power transfer system. In: 2015 IEEE Applied Power Electronics Conference and Exposition (APEC), Charlotte, NC, USA, pp. 597–601 (2015). https://doi.org/10.1109/APEC.2015.7104410
26. Galigekere, V.P., Onar, O., Pries, J., Zou, S., Wang, Z., Chinthavali, M.: Sensitivity analysis of primary-side LCC and secondary-side series compensated wireless charging system. In: 2018 IEEE Transportation Electrification Conference and Expo (ITEC), Long Beach, CA, USA, pp. 885–891 (2018). https://doi.org/10.1109/ITEC.2018.8450163
27. Li, M., Zhang, X., Peng, S., Yang, Z., Yue, M.: Sensitivity analysis of input and output characteristics based on parameters deviation of compensation network in IPT system. In: 2020 IEEE 1st China International Youth Conference on Electrical Engineering (CIYCEE), Wuhan, China, pp. 1–6 (2020). https://doi.org/10.1109/CIYCEE49808.2020.9332782
28. Triviño, A., Fernández, D., Aguado, J.A., Ruiz, J.E.: Sensitivity analysis of component's tolerance in inductively coupled power transfer system. In: 2013 International Conference on Renewable Energy Research and Applications (ICRERA), Madrid, Spain, pp. 806–810 (2013). https://doi.org/10.1109/ICRERA.2013.6749863
29. Li, D., Wu, X., Gao, J., An, C., Gao, W.: Sensitivity analysis of wireless power transmission. Energy Rep. 7(Supplement 7), 138–149 (2021)
30. Song, S., Zhang, W., Jin, Z., Geng, Q.: Analysis of S-S resonance compensation circuit of electric vehicle wireless power transfer system. In: 2020 IEEE 4th Conference on Energy Internet and Energy System Integration (EI2), Wuhan, China, pp. 619–622 (2020). https://doi.org/10.1109/EI250167.2020.9347234
31. Yoo, J.-S., Gil, Y.-M., Ahn, T.-Y.: Steady-state analysis and optimal design of an LLC resonant converter considering internal loss resistance. Energies 15(21), 8144 (2022). https://doi.org/10.3390/en15218144
32. Salehi, N., Martinez-Garcia, H., Velasco-Quesada, G.: A comparative study of different optimization methods for resonance half-bridge converter. Electronics 7(12), 368 (2018). https://doi.org/10.3390/electronics7120368
33. IEC 60063:2015, Preferred number series for resistors and capacitors, International Standard, https://webstore.iec.ch/preview/info_iec60063%7Bed3.0%7Db.pdf
34. Leung, Y.-W., Wang, Y.: Multiobjective programming using uniform design and genetic algorithm. IEEE Trans. Syst., Man, Cybern. C 30(3), 293–304 (2000). https://doi.org/10.1109/5326.885111
35. El Beqal, A., Benhala, B., Zorkani, I.: A Genetic algorithm for the optimal design of a multistage amplifier. Int. J. Electr. Comput. Eng. https://doi.org/10.11591/ijece.v10i1.pp129-138
36. Mostafa, S.S., Horta, N., Ravelo-García, A.G., Morgado-Dias, F.: Analog active filter design using a multi objective genetic algorithm. Int. J. Electron. Commun. 93, 83–94 (2018). https://doi.org/10.1016/j.aeue.2018.06.001
37. Spence, R., Soin, R.S.: Tolerance Design of Electronic Circuits. Cadence Design Syst. Inc. (1997). https://doi.org/10.1142/p032
38. Tarzamni, H., Gohari, H.S., Sabahi, M., Kyyrä, J.: Non-isolated high step-up DC-DC converters: Comparative review and metrics applicability. IEEE Trans. Power Electron. 39(1), 582–625 (2024). https://doi.org/10.1109/TPEL.2023.3264172

How to cite this article: Corti, F., Intravaia, M., Reatti, A., Grasso, F., Grasso, E., Cabrera, A.T.: Component design procedure for LCC-S wireless power transfer systems based on genetic algorithms and sensitivity analysis. IET Power Electron. 17, 906–918 (2024). https://doi.org/10.1049/pel2.12648

APPENDIX

In this section, the coefficients used for the sensitivity analysis are listed:

$$\sigma_1 = 2\omega^2\sigma_3\sigma_4 - 2C_s^2R_L^2\omega^4\left(C_f + C_p - \sigma_6\right)\sigma_4 \tag{A1}$$

$$\sigma_2 = \sigma_4 2 + C_s^2R_L^2\omega^2\sigma_1 \tag{A2}$$

$$\sigma_3 = \sigma_6 - C_p - C_f + L_s\omega^2C_s\left(C_f + C_p\right) + C_fC_pC_s\omega^4\left(M^4 - L_pL_s\right) \tag{A3}$$

$$\sigma_4 = \sigma_{10} + \sigma_9 + \sigma_8 - \sigma_7 + \omega^2C_s(L_s + \omega^2M^2C_f + -C_fC_s\omega^4L_s\left(L_{in} + L_p\right) \tag{A4}$$

$$-C_pC_sL_{in}\omega^4\left(L_s + C_fM^2\omega^2 + C_fL_pL_s\omega^2\right) - 1$$

$$\sigma_5 = \sigma_{10} + \sigma_9 + \sigma_8 - \sigma_7 - 1 \tag{A5}$$

$$\sigma_6 = \omega^2 C_f C_p L_p \tag{A6}$$

$$\sigma_7 = \omega^4 L_{in} L_p C_f C_p \tag{A7}$$

$$\sigma_8 = \omega^2 L_{in} C_p \tag{A8}$$

$$\sigma_9 = \omega^2 L_p C_f \tag{A9}$$

$$\sigma_{10} = \omega^2 L_{in} C_f \tag{A10}$$

$$\sigma_{11} = 2L_{in}\omega^2 \left(\sigma_3\sigma_4 + C_s^2 R_L^2 \omega^2 \sigma_5 \left(\sigma_9 - 1\right)\right) \tag{A11}$$

$$\sigma_{12} = \sigma_9 + \sigma_8 + \sigma_6 - \sigma_7 - 1 \tag{A12}$$

$$\sigma_{13} = \sigma_{10} + \sigma_9 + \sigma_8 + \sigma_6 - \sigma_{10} - \sigma_7 - \omega^4 L_s L_{in} C_s \left(C_f + C_p\right) + -\omega^6 C_f C_p C_s L_{in} \left(M^2 - L_p L_s\right) - 1 \tag{A13}$$

$$\sigma_{14} = 2\sigma_3\sigma_4 - 2C_s R_L^2 \omega^2 \sigma_5 \tag{A14}$$

$$\sigma_{15} = \sigma_4 2 + C_s^2 R_L^2 \omega^2 \sigma_5 \tag{A15}$$

$$\sigma_{16} = C_f \omega^4 \left(L_{in} L_s - M^2\right) - \omega^2 L_s + \omega^4 L_s \left(C_f L_p + C_p L_{in}\right) + + \omega^6 C_f C_p L_{in} \left(M^2 - L_p L_s\right) \tag{A16}$$

$$\sigma_{17} = \sigma_9 + \sigma_8 + \sigma_7 - \sigma_6 + \omega^2 C_s \left(L_s + \omega^2 C_f M^2\right) - \omega^4 C_s L_s \left(\left(L_{in} - L_p\right) C_f - C_p L_{in}\right) + + \omega^6 C_f C_p C_s L_{in} \left(L_p L_s - M^2\right) - 1 \tag{A17}$$

$$\sigma_{18} = 2\omega^2 \left(\sigma_3\sigma_4 + \sigma_5 C_s^2 R_L^2 \omega^2 \left(L_{in} + L_p - \sigma_6\right)\right) \tag{A18}$$

$$\sigma_{19} = \sigma_4^2 + C_s^2 R_L^2 \omega^2 \sigma_5^2 \tag{A19}$$